Journal of Power Sources 196 (2011) 5045–5052

Contents lists available at ScienceDirect

Journal of Power Sources

journal homepage: www.elsevier.com/locate/jpowsour

# Diagnosis of MEA degradation under accelerated relative humidity cycling

S. Vengatesan[a,b], Michael W. Fowler[a,*], Xiao-Zi Yuan[b], Haijiang Wang[b]

[a] Department of Chemical Engineering, University of Waterloo, 200 University Avenue West, Waterloo, ON, Canada N2L 3G1
[b] Institute for Fuel Cell Innovation, National Research Council Canada, 4250 Wesbrook Mall, Vancouver, BC, Canada V6T 1W5

ARTICLE INFO

*Article history:*
Received 23 November 2010
Received in revised form 25 January 2011
Accepted 27 January 2011
Available online 4 March 2011

*Keywords:*
Durability
MEA degradation
Polymer electrolyte membrane fuel cells
RH cycling
Selective permeability

ABSTRACT

The objective of this work is to identify the failure mode diagnosis protocols for polymer electrolyte membrane (PEM) fuel cells with the use of accelerated testing conditions. The single cells used in this work were constructed using commercial Ion Power® membrane electrode assemblies (MEAs) and the performance degradation was studied under accelerated dynamic reactant relative humidity (RH) conditions. The influence of RH on cell performance was investigated, and a strong dependence of degradation with respect to relative humidity was found. RH cycling was seen to not only cause the gradual decrease in performance at the beginning of cell operation, but it was also related to the rapid decline in performance observed after 330 h operation. This change in degradation rate is seen a change in the material degradation failure mechanism at this point in the operational history of the cell. The increase in cell resistance, membrane crossover, fluoride release rate and decrease in electrochemical surface area (ESA) were also observed with time, and these results were correlated to change in degradation rate. Infra-Red (IR) imaging of an aged MEA was utilized to show varying temperature profiles and outline the possibility of cracks, tears or pinholes in the membrane.



## 1. Introduction

Durability of materials and cell components is a major concern for the successful commercialization of polymer electrolyte membrane (PEM) fuel cells in automotive and portable applications [1,2]. Since material degradation and lifetime change in a fuel cell are fully dependant on the operating conditions [3–7], the challenge of durability issues is mainly focused on the detailed understanding of failure modes and degradation mechanisms, as well as the systematic approaches to mitigate these problems [8]. Among the fuel cell components, the membrane electrode assembly (MEA) is considered to be the integral element, since it decides the maximum power density obtained from the electrochemical reaction. Furthermore, the MEA, comprised of an anode and a cathode together with a membrane, is the main site for degradation during cell operation under dynamic conditions [9–12].

Much of the published research on PEM fuel cells is focused on performance degradation, damage to the cell components and failure modes [5,11,13–15]. To evaluate the lifetime of a fuel cell, there are two methods of testing: steady state lifetime tests or accelerated stress tests. Accelerated stress tests are more convenient to execute since they significantly reduce the experiment time while still providing valuable degradation information [16,17]. The accelerated stressors, such as open circuit voltage (OCV) operation [3], load/potential cycling [5], and freeze/thaw cycling [4,6] are the most common stressors used to study fuel cell degradation and failure modes. On the other hand, these test procedures can induce failure to the system that may not be related to actual operational conditions, which makes it hard to understand the exact causes and failure modes of degradation. However, accelerated testing with periodic observation of cell characteristics, such as performance, cell resistance, and catalyst activity, and systematic analysis of the results, may be used to explore these failure modes further.

The polymer electrolyte membrane in a fuel cell is the component that ensures proton conduction. It also acts as a gas and electrical barrier between the anode and the cathode. The polymer membrane undergoes various degradation modes, including chemical, mechanical and thermal degradation under harsh operation conditions [18,19]. Unfortunately, membrane failure often occurs by a combination of these degradation modes when the fuel cell is subjected to specific operating conditions, making determination of the cause of failure difficult. Investigation into each of the individual degradation mode, under differing operating conditions, would clarify the impact of each mode on cell degradation and failure that allows material design improvements. Among the failures, membrane mechanical failure, which results in irreparable damages to the membrane, is considered a principal cause of early failures in fuel cell testing. Relative humidity (RH) cycling is one of many operational parameters that contribute to mechanical failure

* Corresponding author. Tel.: +1 888 4567x33415; fax: +1 519 746 4979.
*E-mail addresses:* mfowler@cape.uwaterloo.ca, mfowler@uwaterloo.ca (M.W. Fowler).

0378-7753/$ – see front matter © 2011 Elsevier B.V. All rights reserved.
doi:10.1016/j.jpowsour.2011.01.088

of the membrane; however, RH also plays a vital role in a fuel cell performance since the proton conductivity of the membranes in a perfluorosulfonic acid (PFSA) based fuel cell strongly depends upon level of membrane hydration [20]. Thus, fuel cells are operated to certain level of humidified conditions to achieve high performance.

In the literature, many researchers examined the influence of RH changes on PEM fuel cell performance [14,21–24]. The results indicated that low RH could strongly degrade fuel cell performance by increasing the membrane and catalyst layer resistance and decreasing the overall electrode kinetics. In addition, RH changes can cause material degradation, especially membrane mechanical degradation [25]. Therefore, RH cycling can be used as an effective stressor to induce membrane mechanical failure allowing the subsequent performance degradation mechanisms and failure modes to be studied. In the same manner, some authors explored fuel cell degradation under humidity cycling [13,26,27]. From their results, the membrane undergoes series of stress/strain cycles and elastic-plastic deformation during RH cycling. This induced non-uniform stresses along the in-plane direction and caused sudden mechanical failure of the membrane. However, their results were not correlated with other diagnostic tests, and little forensic examination is reported.

In this work, MEA degradation with a main emphasis on identifying the failure modes under accelerated conditions will be studied using symmetric humidity cycling (same anode/cathode humidity). For this, the full cell will be operated with dynamic hydration cycling by switching the RH between high and extremely low levels. The changes in cell performance, resistance, electrochemical surface area (ESA), $H_2$ crossover were periodically observed during the cycling and humidified conditions in order to investigate the influence of RH cycling on normal MEA degradation. Extensive ex situ analyses were carried out periodically during the testing to study the component failure. Selective gas permeability measurements were also conducted after periodic intervals of cell testing to observe the membrane crossover. Water samples from anode and cathode outlets were analyzed at periodic time intervals to check the fluoride content as an indicator of PFSA membrane degradation. A post-analysis of degraded MEA samples was conducted to observe the membrane failures and MEA morphological changes.

## 2. Experimental

### 2.1. Membrane electrode assembly (MEA) and accelerated cell testing

The MEA used in this study was manufactured by Ion Power Inc. The single cell was assembled with a catalyzed Ion Power® NR 212 membrane with 0.3 mg Pt $cm^{-2}$, SGL 30BC GDLs (both anode, cathode), composite bipolar plates (Dana Corp.), copper current collectors, and stainless steel end plates. The active area of the cell was 50 $cm^2$, and the cell temperature was maintained constantly at 75 °C using the water coolant plate for all the single cell testing. $H_2$ and air were fed into anode and cathode either at constant or stoichiometric flow rates, and the cell was run at atmospheric pressure.

The accelerated cell operation was performed by cycling the RH between saturated (100% RH) and dry gas conditions using a feed stream bypass to ensure rapid transfer of the cycle. As shown in Fig. 1, the cell was run at a fully humidified state and at cycling conditions alternately, with the cell performance being observed periodically at both conditions. During the RH cycling and humidified conditions, the cell was operated at the current density of 300 mA $cm^{-2}$. $H_2$ and air were fed into anode and cathode at the stoichiometric ratio of 1.5 and 2.0, respectively.

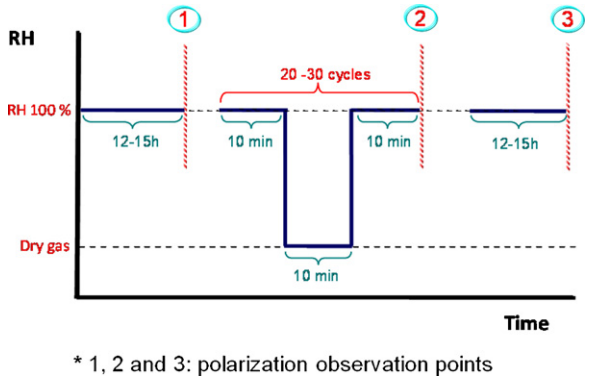


**Fig. 1.** Schematic diagram of RH cycling experiment operating conditions.

### 2.2. Electrochemical testing

*I–V* characteristics of the single cell were performed periodically during the endurance testing using an electronic load RBL 232 (TDI electronic devices). As shown in Fig. 1, three operational conditions were chosen in this study. Points 1 and 3: the cell under humidified condition before and after RH cycling experiments; point 2: cell immediately after the cycling experiments. The impedance of the single cell was measured using a Solartron impedance analyser (Model-SI 1260) with a potentiostat/galvanostat (Model-273). The experiment was performed at a constant potential of 0.85 V with an amplitude of 5 mV. The frequency was scanned from 10 mHz to 10 kHz. Cyclic voltammetry (CV) and linear sweep voltammetry (LSV) experiments were done using the potentiostat/galvanostat (Model-273). For CV experiments, the potential was scanned in the range of 0.05–1.2 V vs. NHE at a scan rate of 20 mV $s^{-1}$; whereas, the LSV experiments have been conducted in the potential range of 0.05–0.6 V vs. NHE with a scan rate of 2 mV $s^{-1}$.

### 2.3. Selective gas permeability testing

The selective permeability testing of gases (He, $N_2$, Ar) through the MEA was conducted at regular time intervals after the MEA was run under RH cycling conditions consistent with the method employed by Kundu et al. [30]. This information was gathered to see the change in membrane crossover throughout the durability testing and investigate the membrane failure modes. During this experiment, the cell was taken off the test station, and selective gases were fed into anode side of the cell and the gas flux across the membrane was measured at the cathode. The apparent permeability ($P_M$) of the membrane was calculated using Fick's law (Eq. (1)):

$$N_A = \frac{P_M(P_I - P_{II})}{d} \quad (1)$$

$P_I$ and $P_{II}$ are the partial pressures of the analysis gas at either side of the membrane; $N_A$ is the flux of gas molecules across the membrane with a finite thickness ($d$). It is assumed that the gas flux through the membrane will increase if the membrane thickness changes due to thinning, and/or the presence of membrane pinholes, tears, or cracks.

### 2.4. Fluoride analysis measurements

The fluoride content of the water samples collected from the anode and cathode at regular time intervals was analyzed using an Ion Chromatograph (Dionex DX 500) with a conductivity detector. The analytical column used to separate the fluoride ions from other anions was a Dionex AS17 plus AG17 guard column, and 20 mM

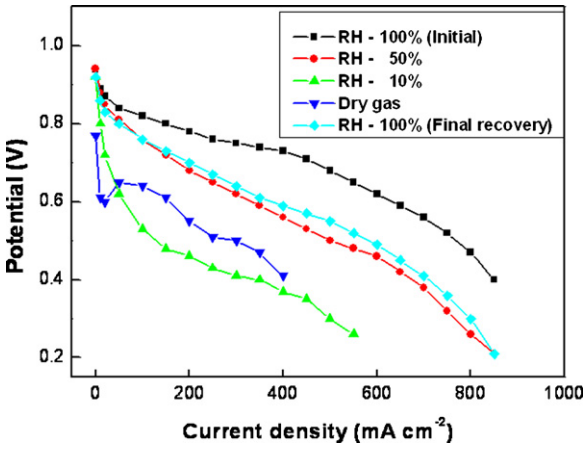


**Fig. 2.** Polarization curves of the MEA at different RH values; $T_{cell}$ = 75 °C.

NaOH was used as the eluent. The minimum detectable limit of fluoride ions in the sample was 0.011 mg $L^{-1}$.

### 2.5. Post-analysis of degraded MEA

The MEA was post-analyzed, using an Infra-Red camera (InfraTech GmbH) after the endurance testing, to identify thinning, hotspots, pinholes and cracks in the membrane. For this, the degraded MEA was removed from the cell and installed into a dummy cell in which the cathode side was exposed to the IR camera. Hydrogen gas was passed on the anode side at a minimum flow rate and the crossover hydrogen, through the thinned areas and pinhole in the membrane, encountered the oxygen at the cathode side, which produced heat due to the direct combustion of $H_2$ and $O_2$ in presence of the Pt catalyst. The IR camera observed the temperature variation along the MEA and the temperature profile created was compared with the temperature profile obtained for a fresh MEA.

## 3. Results and discussion

### 3.1. Effect of relative humidity on cell performance

Since the proton conductivity of PFSA membranes is a function of its water content, changes in RH can cause detrimental effect on cell performance. To see the influence of RH on cell performance, the cell was operated at different RHs (100%, 50%, 10% and dry gas) and the single cell performances are shown in Fig. 2. The cell was run for a sufficient amount of time (~12 h) to ensure the stabilization of the cell at each RH condition before taking the *I–V* curves. The polarization curves were recorded from low to high current at all RH conditions, except for the 'dry gas' operation, which was done from high to low current. From the figure, it can be seen that the MEA showed maximum performance at fully humidified state (100% RH), and that the performance decreased significantly as the RH was reduced to 50%. Further reduction of the RH (i.e., 50% to 10%), led to a drastic decrease in cell performance. This decrease is the inevitable outcome of insufficient hydration of the membrane and ionomer in the catalyst layer, which leads to high cell resistance at low RH values. To see the influence of dry gas on performance, the cell was also operated using dry reactant gases without external humidification. Since the potential dropped too rapidly from OCV, the polarization curve for the dry operation was carried out from a high current to ensure the membrane was at a sufficient hydration level. From Fig. 2, it can be seen that the polarization curve is unstable as it approaches low voltage. This is due to uneven water content in the membrane during dry gas operation. In addition, the recovery of cell performance was evaluated after switching the RH from dry gas to fully humidified conditions (100%), and it can be seen that the performance could not fully recover even after allowing the cell adequate time. This confirmed irreversible changes in the MEA performance during low RH operations.

The impedance spectra and cyclic voltammograms of the cell at different RHs are depicted in Fig. 3a and b. From the impedance spectra, it can be seen that the low frequency/charge transfer resistance increased slightly as the RH was reduced from 100% to 50%. This shows the inefficient proton transfer from the catalyst layer to membrane at low humidification. Additionally, further decrease in RH to 10% drastically increased both low and high frequency resistances. Since the high frequency resistance is mainly considered the ohmic resistance of the cell, the increase in this resistance may be connected to the membrane proton conductivity loss at low hydration (the proton conduction mechanism is believed to happen with water molecules). Moreover, the decrease in ohmic resistance observed when the cell was reversed to 100% RH, apart from the slight increase in low frequency resistance, demonstrates that the membrane could resume its proton conductivity once sufficient hydration was re-administered.

In the cyclic voltammograms, the hydrogen desorption area (0.0–0.4 V vs. NHE) is used as a measure of active surface area of the catalyst available for electrochemical reactions. In the graph, as the RH was reduced, the desorption area decreased due to poor catalyst–ionomer connectivity. Based on these results, the RH studies confirmed the strong dependence of cell performance on relative humidity, and constructed the basis for designing the RH cycling experiments.

### 3.2. Effect of RH cycling on MEA performance degradation

As shown in Fig. 1, the RH of the cell was cycled between the two extreme RH values, 100% and dry gas, during the cell degrada-

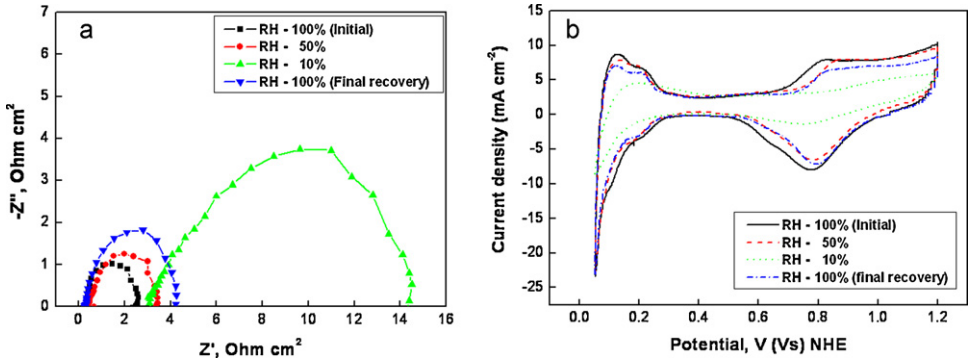


**Fig. 3.** (a) Impedance curves of MEA at 0.85 V; (b) cyclic voltammograms of MEA at different RHs; scan rate = 20 mV $s^{-1}$.

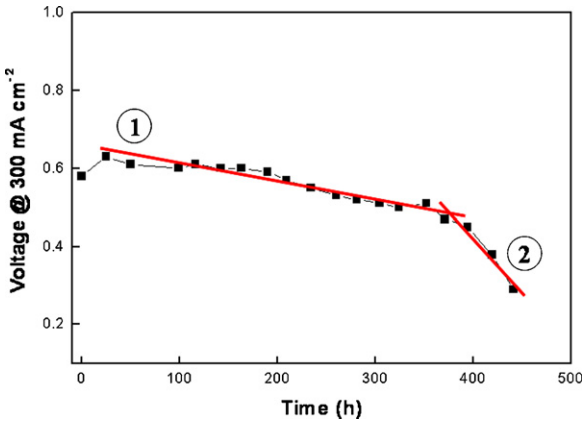


**Fig. 4.** Voltage degradation with time under RH cycling accelerated aging conditions.

tion studies. The influence of RH cycling on the normal degradation of the MEA under humidified conditions was then studied. Fig. 4 shows the voltage degradation with time under humidified conditions in which the RH cycling was done at periodic time intervals. As is evident from Fig. 4, the voltage decreased gradually until 330 h of operation and then was seen to rapidly decline after about 350 h. The slope of the voltage degradation curve changed significantly at this point (i.e. slope 2). This abrupt change in voltage indicates the failure of fuel cell components due to hydration cycling, likely pinhole formation that will be discussed in further detail in subsequent sections.

Fig. 5a shows the changes in MEA performance under humidified conditions before and after the RH cycling experiments (Fig. 1: *I–V* points 1 and 3). From the figure, there is a gradual decrease in performance until 352 h of cell operation, and then a considerable decrease in performance observed after 352 h. The gradual decrease is likely to be the result of catalyst layer degradation and gradual membrane thinning. The changes in the catalyst layer were likely accelerated in the catalyst–ionomer interface due to low humidity operation. On the other hand, the marked decrease in OCV at 352 h of operation indicates that some other type of failure mode has arisen due to a change or damage to the MEA components.

Since the decrease in OCV mostly occurred due to reactant crossover, it can be assumed the failure mode that manifested at this time was failure of the MEA. There is a rapid decrease in OCV observed after 352 h, accompanied by the decrease in performance. This could have arisen from the high crossover of gases through the membrane causing the subsequent loss of performance efficiency. This would indicate the formation of a significant pinhole. To observe the fatal degradation points and failure modes intensely, the performance of the cell was also observed immediately after the RH cycling (Fig. 1: *I–V* point 2) and illustrated in Fig. 5b. As shown, there is a marginal decrease in performance observed up until the 240th cycle (334 h). After 240 cycles, there is a rapid decrease in cell performance and OCV, which is in agreement with the performance results shown in Fig. 5a. Because of the sequential nature of performing the different diagnosis tests the exact time of the failure cannot be specified, and different diagnostic tests revealed the failure a slight different hours of operation.

### 3.3. Diagnosis of failure modes: in situ analysis

#### 3.3.1. Impedance

The impedance curves of the cell under humidified condition and immediately after cycling are shown in Fig. 6a and b. Though the change in high frequency resistance is not clearly visible, the low frequency resistance increased to a large extent with time. The reasons for this might be explained as follows: since proton conduction is facilitated with water molecules, insufficient water would cause poor proton transfer at the catalyst–ionomer interface. As a result, the poor contact between catalyst particles and ionomer might have reduced the effective charge transfer at low RH. On the contrary, the sudden decrease in the low frequency resistance, at 382 h (Fig. 6b) and 419 h (Fig. 6a), which appears suddenly, is a strong indicator of membrane failure via pinhole formation.

The low frequency resistance (LFR) and the high frequency resistance (HFR), calculated from the impedance curves, were plotted with time, and are shown in Fig. 7. The HFR of the cell increased steadily with time until the cell reached the critical degradation point (i.e., 334 h). After this point, the HFR decreased drastically, which is indicative of the possibility of a short circuit inside the MEA due to membrane thinning and/or crack formation where a short can be manifested. On the other hand, the drastic increase in LFR occurred unevenly with time, which is mainly assigned to the collapse of the catalyst–ionomer interface. From this observation, we can infer that it is the ionomer in the catalyst layer that undergoes changes/degradation first during RH cycling experiments, rather than the membrane.

#### 3.3.2. Voltammetry

The cyclic voltammograms, shown in Fig. 8, displayed the characteristic peaks of an electrochemical redox process occurring on a Pt/C catalyst. From Fig. 8a and b, the hydrogen desorption area, which is a measure of electrode surface area, decreased as the cell operation time increased. However, there is an abrupt change in the voltammogram that deviates from normal behaviour, which is observed after 240 cycles (Fig. 8b). This indicates the possible existence of a short circuit in the MEA caused from membrane thinning, tears or cracks. After this stage, it was unworkable to

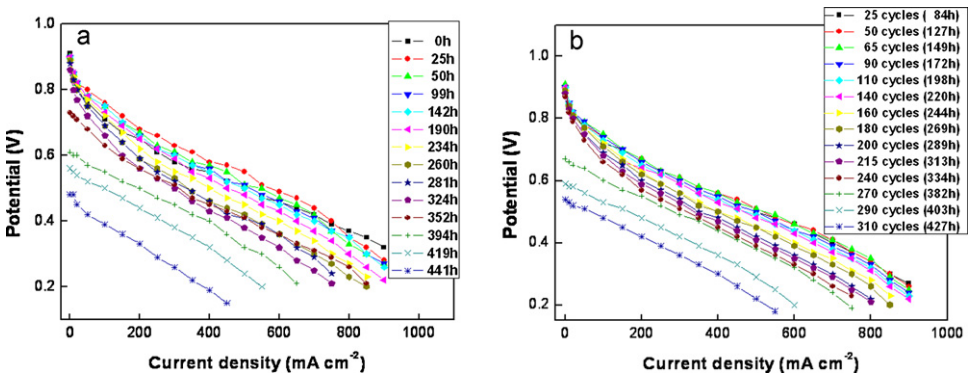


**Fig. 5.** *I–V* characteristics of the single cell (a) under humidified condition, before and after RH cycling operation; (b) immediately after cycling experiments; $T_{cell}$ = 75 °C; $H_2$/air stoichiometry = 1.5/2.0.

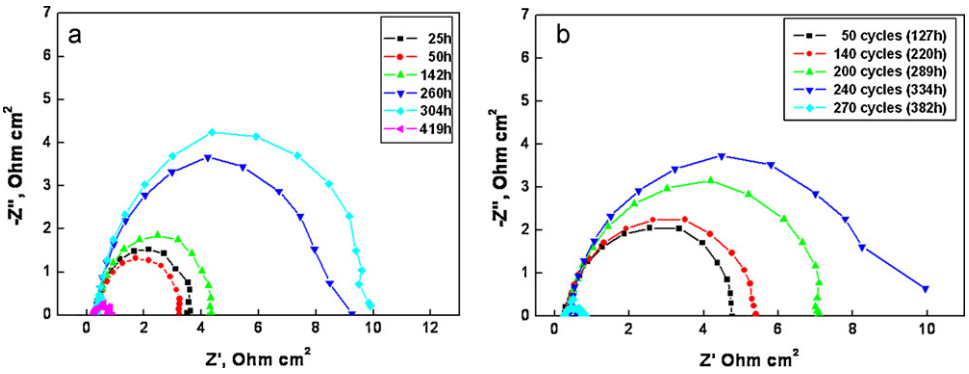


**Fig. 6.** Impedance curves of MEA at 0.85 V (a) under humidified conditions, before and after the RH cycling experiments; (b) immediately after the RH cycling operation.

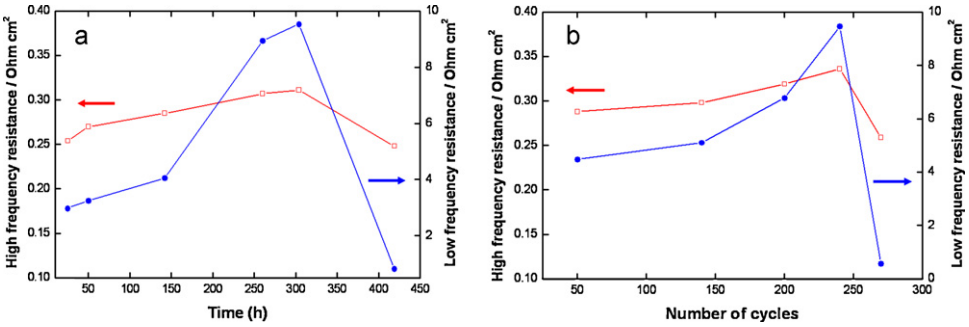


**Fig. 7.** HFR and LFR changes (a) under humidified conditions, before and after cycling experiments; (b) immediately after the RH cycling operation.

observe cyclic voltammograms as the current exceeded the limit of the instrument.

The hydrogen crossover results from linear sweep voltammetry (LSV), shown in Fig. 9, further confirmed these findings. Hydrogen crossover current, which is mainly contributed by the hydrogen that crosses over from anode to cathode, and this diagnostic is the strongest evidence of membrane failure, including thinning, pinholes and/or cracks [12]. From Fig. 9a, a marginal increase in crossover current density can be seen until the cell reaches 304 h of operation, likely due to membrane thinning. However, after 240 cycles (334 h) in Fig. 9b, the cell exhibited high hydrogen crossover, which caused a sudden decrease in cell efficiency. According to Cheng et al. [28], the $H_2$ crossover strongly depends on the cell temperature and humidity and increases at high temperature and low RH. Since the membrane is exposed to higher temperatures during the dry cycles in this study, the membrane crossover is expected to increase as the number of cycling increases.

The electrochemical surface area (ESA), calculated from cyclic voltammograms and $H_2$ crossover current from linear sweep voltammograms (LSV), was plotted with time and is shown in Fig. 10. The ESA decreased almost linearly with time, showing the changes in electrode microstructure. In an earlier study, Uribe et al. [29] also found a decrease in ESA as the humidity level changed. Uribe et al. suggested that, at low hydration of the ionomer, the hydrophobic domain of the ionomer came into contact with the catalyst surface rather than the hydrophilic groups, which reduced the three-phase boundary.

As can be seen, $H_2$ crossover current, which gives the information about membrane failure, does not change significantly up to 300 h of operation. However, an abrupt increase in $H_2$ crossover occurred after 240 cycles (334 h). This finding shows that the membrane might have experienced integrity failure (pinhole or crack) damage at this stage due to the fatigue stresses imposed by humidity cycling. The increase in hydrogen crossover is much more pronounced immediately after hydration cycling event (Fig. 10b) indicating that small integrity failures and pinholes contribute less to the crossover during fully humidified conditions as the membrane may swell to seal these failures. The MEA post analysis

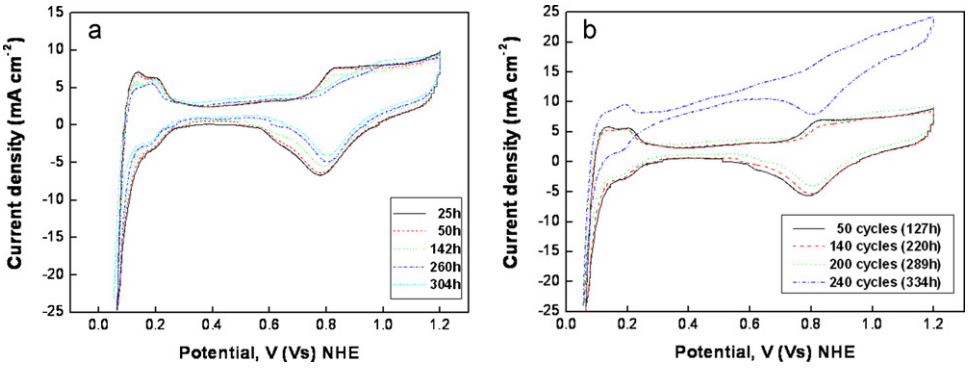


**Fig. 8.** Cyclic voltammograms of the MEA (a) under humidified conditions, before and after cycling operation; (b) immediately after the RH cycling event; scan rate = 20 mV $s^{-1}$.

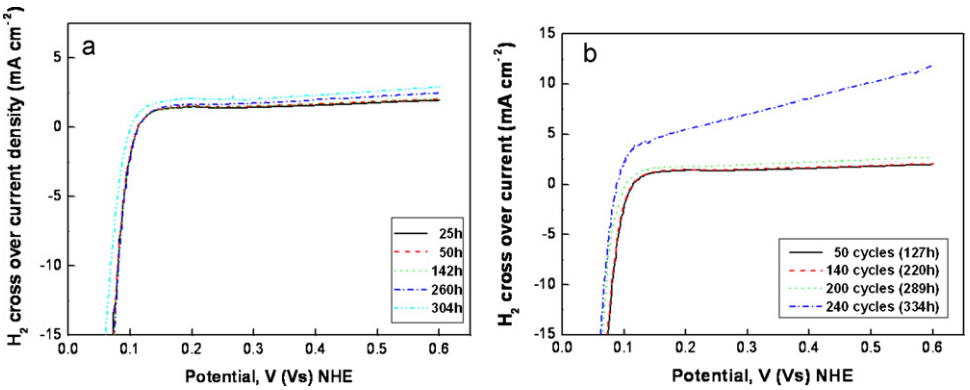


**Fig. 9.** LSV curves of the MEA (a) operated under humidified conditions, before and after RH cycling; (b) immediately after humidity cycling; scan rate = 2 mV $s^{-1}$.

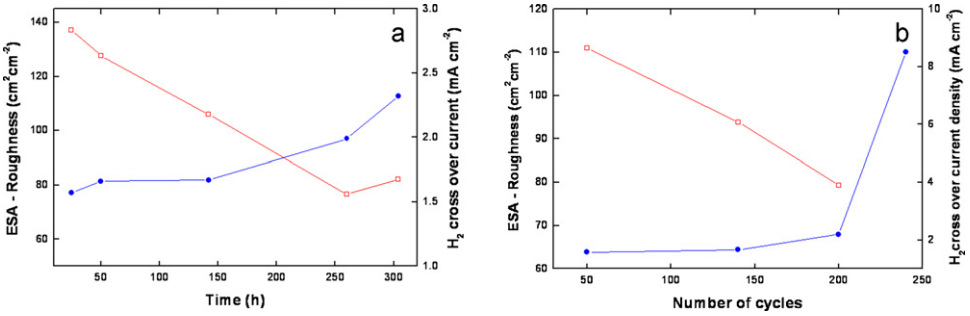


**Fig. 10.** ESA and $H_2$ crossover changes (a) under humidified conditions; (b) under cycling conditions.

results, which will be discussed in a later section also correlated with this diagnosis of pinhole formation.

### 3.4. Diagnosis of failure modes: ex situ analysis

#### 3.4.1. Selective permeability of gases

Selective permeability of gases through the membrane is an easy and viable method to investigate membrane failure during fuel cell operation. Since membrane mechanical integrity failures predominantly associated with the development of pinholes, rips, tears and cracks, an sudden increase in permeability may be expected during testing. The inert gases, $H_2$, $N_2$ and Ar, were chosen for this work's permeability experiments. Using different gases and their selectivity, one can distinguish whether the permeation is related with solution or Knudson behaviour [30]. Fig. 11 shows the permeability of gases with time. In our experiment, we observed almost no gas permeability through the membrane until 250 h of testing. By 350 h of testing, the permeability had started increasing slowly (not noticeable in the figure), which is identified as the driving point for membrane failure. After 350 h, a sudden increase in permeability is observed, which displays critical damage to the membrane. Since the permeation of all three different gases is the same, the mass transfer is not related with Knudson behaviour and that indicates the pores are of a significant size and formed quickly. The observed results are also similar to the LSV results in which electrochemical $H_2$ crossover current increased drastically after 334 h of operation.

#### 3.4.2. Fluoride analysis

The PFSA membranes and ionomer undergo degradation during cell operation to produce degradation products, such as fluoride ions, sulfates, and small polymer end groups [15]. Consequently, analysis of water from the cell outlets may be essential in revealing the degradation level of the membrane and ionomer in the catalyst layer. For this, water samples were collected from the anode

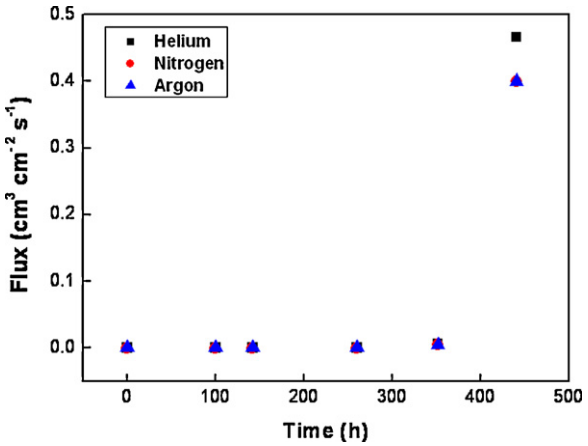


**Fig. 11.** Change in permeability of gases through MEA with time.

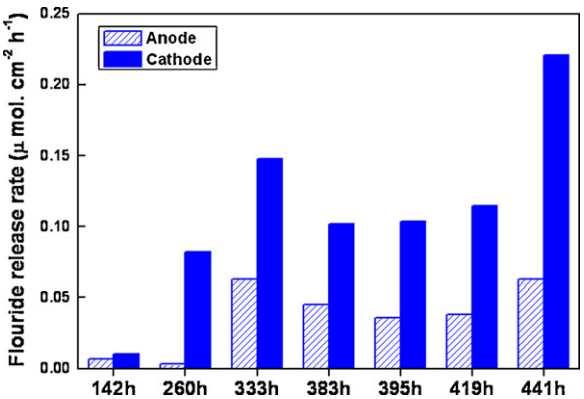


**Fig. 12.** Change in fluoride release rate with time.

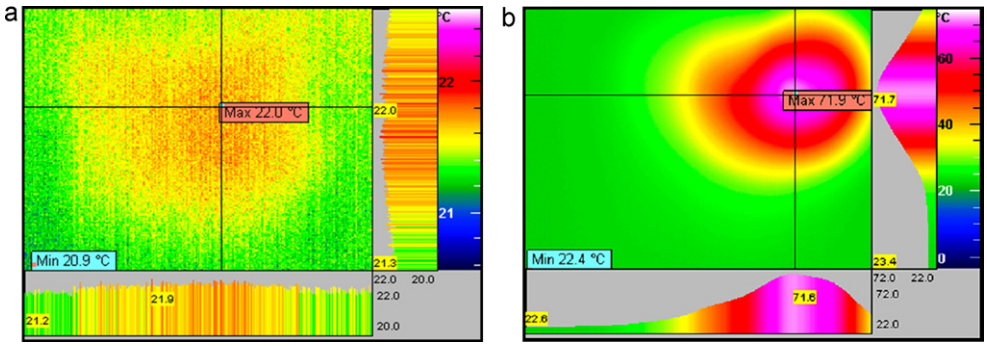


**Fig. 13.** Temperature profile of (a) fresh MEA; (b) degraded MEA using IR camera.

and cathode outlets at periodic time intervals during the RH cycling experiments. The water samples were then analyzed using an Ion chromatograph and the cumulative fluoride release rates at the anode and cathode exits were plotted with time in Fig. 12. From the figure, the cathode fluoride release rate roughly increased with time, while the anode release rate showed an irregular pattern. The reason for this could be explained by the transportation of the fluoride ions across the membrane with water from anode to cathode during the electro-osmotic process. The exceptional spike, appearing at 330 h of operation, gives further evidence of a high level of degradation to the membrane and/or ionomer in the catalyst layer during that stage. It is likely that associated with the pinhole formation and increased hydrogen crossover that lead to accelerated degradation of the membrane material in the localized region of the failure. This is mainly due to the spike in temperature from the direct hydrogen oxidation at this location.

Post-analysis of the MEA components is a good diagnostic method for studying the material failure, morphological and microstructural changes. The temperature profiles of the fresh and degraded MEAs, created using the IR camera, are shown in Fig. 13.

The variation in the temperature profile gives an idea about the membrane failure. As expected, there is no temperature variation observed with the fresh MEA due to the absence of any perforation. On the other hand, a non-uniform temperature distribution and a hot spot (at the right corner of the image), with the maximum temperature of 71.9 °C, are observed for the degraded MEA. In the MEA, this hot-spot region is identified as the area of the anode inlet. In general, the anode is more dehydrated than the cathode during dry gas operation due to the electro-osmotic process that takes the water from anode to cathode. Therefore, these results are fully inline with our expectations that the anode inlet region is more susceptible to fatigue stresses and gas crossover.

It is very obvious that the abrupt change in the fuel cell occurred after 330 h of operation, from a number of diagnostics associated with both in situ and ex situ analysis results. Since the IR camera results revealed damage in the membrane, membrane failure is likely to be the failure mode of associated MEA degradation. Hence, the membrane failure mechanisms such as thinning, pinhole and/or crack formation could be the cause for this failure. According to Kusoglu et al. [13], the membrane undergoes fatigue stresses due to swelling anisotropy under hydration–dehydration cycles, and these uneven stresses also contribute to tearing/cracking in the membrane. In this work the hydration cycling was used to accelerate the integrity failure of the MEA, in order to highlight the correlation of a number of diagnostic techniques for PEM fuel cells.

## 4. Conclusions

The single cells were operated using commercial Ion Power® MEAs, and the performance and material degradation were studied under accelerated RH cycling conditions. The cell performance decreased gradually during initial cell endurance testing, and there was a sudden performance decline observed after 330 h of operation. This performance failure has been correlated with a number of different full cell diagnostics, specifically electrochemical methods such as AC impedance spectroscopy and cyclic voltammetry, hydrogen crossover measurements, changes in the slope of the degradation curve. Mainly the voltage degradation slope changed abruptly at the end of life testing, and an increase in cell resistance and decrease in ESA with the number of cycling was revealed by impedance and CV results. Furthermore, the increase in $H_2$ crossover rate correlated with the other diagnostic tests to indicate that pinhole formation in the MEA was the likely cause for the abrupt performance decay.

The selective permeability results showed a rapid increase in gas flux after 330 h of testing which further correlated with the possibility of membrane failure. The fluoride analysis results demonstrated the level of polymer membrane degradation and exhibited an irregular fluoride release rate over time with high fluoride release both at 330 h and at the end of life testing.

IR imaging diagnostic results also correlated with other diagnostic tools executed in this study to explore the possibility of membrane thinning, presence of pinholes or tears/cracks, which can be attributed to the mechanical stress induced on the membrane during RH cycling. Based on the results, it is concluded that the failure mode of MEA likely originated from membrane failure that might be due to the uneven mechanical stresses imposed by RH cycling. This work has shown that a number of diagnostics tests can be correlated with a specific failure mode in PEM fuel cell operation.

## Acknowledgements

The authors acknowledge the NRC-Helmholtz Joint Research Program, as well as the NRC-University of Waterloo research program for their financial support.

## References

[1] F.A.d. Bruijn, V.A.T. Dam, G.J.M. Janssen, Fuel Cells 8 (1) (2008) 3–22.
[2] R. Borup, J. Meyers, B. Pivovar, Y.S. Kim, R. Mukundan, N. Garland, D. Myers, M. Wilson, F. Garzon, D. Wood, P. Zelenay, K. More, K. Stroh, T. Zawodzinski, J. Boncella, J.E. McGrath, M. Inaba, K. Miyatake, M. Hori, K. Ota, Z. Ogumi, S. Miyata, A. Nishikata, Z. Siroma, Y. Uchimoto, K. Yasuda, K.-i. Kimijima, N. Iwashita, Chemical Reviews 107 (10) (2007) 3904–3951.
[3] S. Kundu, M. Fowler, L.C. Simon, R. Abouatallah, Journal of Power Sources 182 (1) (2008) 254–258.
[4] Q. Guo, Z. Qi, Journal of Power Sources 160 (2) (2006) 1269–1274.
[5] D. Liu, S. Case, Journal of Power Sources 162 (1) (2006) 521–531.
[6] J. Hou, H. Yu, S. Zhang, S. Sun, H. Wang, B. Yi, P. Ming, Journal of Power Sources 162 (1) (2006) 513–520.
[7] S.J.C. Cleghorn, D.K. Mayfield, D.A. Moore, J.C. Moore, G. Rusch, T.W. Sherman, N.T. Sisofo, U. Beuscher, Journal of Power Sources 158 (1) (2006) 446–454.
[8] S. Zhang, X. Yuan, H. Wang, W. Mérida, H. Zhu, J. Shen, S. Wu, J. Zhang, International Journal of Hydrogen Energy 34 (1) (2009) 388–404.

[9] M. Schulze, A. Schneider, E. Gülzow, Journal of Power Sources 127 (1–2) (2004) 213–221.
[10] J. Xie, D.L. Wood III, K.L. More, P. Atanassov, R.L. Borup, Journal of the Electrochemical Society 152 (5) (2005) A1011–A1020.
[11] S.D. Knights, K.M. Colbow, J. St-Pierre, D.P. Wilkinson, Journal of Power Sources 127 (1–2) (2004) 127–134.
[12] M. Inaba, T. Kinumoto, M. Kiriake, R. Umebayashi, A. Tasaka, Z. Ogumi, Electrochimica Acta 51 (26) (2006) 5746–5753.
[13] A. Kusoglu, A.M. Karlsson, M.H. Santare, S. Cleghorn, W.B. Johnson, Journal of Power Sources 170 (2) (2007) 345–358.
[14] C. Song, C. Jensen Chua, Y. Tang, J. Zhang, J. Zhang, J. Li, K. Wang, S. McDermid, P. Kozak, International Journal of Hydrogen Energy 33 (11) (2008) 2802–2807.
[15] K. Teranishi, K. Kawata, S. Tsushima, S. Hirai, Electrochemical and Solid-State Letters 9 (10) (2006) A475–A477.
[16] M.J. Heneka, E. Ivers-Tiffee, ECS Transactions 1 (8) (2006) 377–384.
[17] M. Hicks, D. Pierpont, P. Turner, T. Watschke, ECS Transactions 1 (8) (2006) 229–237.
[18] A. Collier, H. Wang, X. Zi Yuan, J. Zhang, D.P. Wilkinson, International Journal of Hydrogen Energy 31 (13) (2006) 1838–1854.
[19] N. Ramaswamy, N. Hakim, S. Mukerjee, Electrochimica Acta 53 (8) (2008) 3279–3295.
[20] S. Vengatesan, H.J. Kim, E.A. Cho, S.U. Jeong, H.Y. Ha, I.H. Oh, S.A. Hong, T.H. Lim, Journal of Power Sources 156 (2) (2006) 294–299.
[21] J. Zhang, Y. Tang, C. Song, Z. Xia, H. Li, H. Wang, J. Zhang, Electrochimica Acta 53 (16) (2008) 5315–5321.
[22] H. Xu, H.R. Kunz, J.M. Fenton, Electrochimica Acta 52 (11) (2007) 3525–3533.
[23] J. Zhang, Y. Tang, C. Song, X. Cheng, J. Zhang, H. Wang, Electrochimica Acta 52 (15) (2007) 5095–5101.
[24] M.M. Saleh, T. Okajima, M. Hayase, F. Kitamura, T. Ohsaka, Journal of Power Sources 164 (2) (2007) 503–509.
[25] S. Kundu, L.C. Simon, M. Fowler, S. Grot, Polymer 46 (25) (2005) 11707–11715.
[26] V.A. Sethuraman, J.W. Weidner, A.T. Haug, L.V. Protsailo, Journal of the Electrochemical Society 155 (2) (2008) B119–B124.
[27] X. Huang, C. Russo, Y. Zou, R. Solasi, K. Reifsnider, D. Condit, ECS Meeting Abstracts 701 (7) (2007) 402–1402.
[28] X. Cheng, J. Zhang, Y. Tang, C. Song, J. Shen, D. Song, J. Zhang, Journal of Power Sources 167 (1) (2007) 25–31.
[29] F.A. Uribe, T.E. Springer, S. Gottesfeld, Journal of the Electrochemical Society 139 (3) (1992) 765–773.
[30] S. Kundu, M.W. Fowler, L.C. Simon, Journal of Power Sources 180 (2) (2008) 760–766.